

Composite Picture of the Charge Carriers in the Superconducting Layered Cuprates

Y. H. Kim¹, P. H. Hor^{2,3}, X. L. Dong^{3,4}, F. Zhou⁴, Z. X. Zhao⁴, Y. S. Song³, and W. X. Ti⁴

¹Department of Physics, University of Cincinnati, Cincinnati, Ohio 45221-0011, USA

²Department of Physics, University of Houston, Houston, Texas 77204-5005, USA

³Texas Center for Superconductivity, University of Houston, Houston, Texas 77204-5002, USA

⁴National Laboratory for Superconductivity, Institute of Physics and Center for Condensed Matter Physics, Chinese Academy of Sciences, P.O. Box 603, Beijing 100080, P.R. China

Through the far-infrared studies of $\text{La}_{2-x}\text{Sr}_x\text{CuO}_4$ single crystals for $x = 0.063, 0.07, 0.09,$ and 0.11 , we find that only $\sim 0.2\%$ of the total holes participated in the nearly dissipationless normal state charge transport and superconductivity. These free carriers are massively screened by the rest of the holes bound in an electronic lattice (EL) state. Our findings lead us to a composite picture of the charge system where the free carriers are coupled to and riding on the EL. This unique composite system of charge carriers provides further insights into the understanding of the cuprate physics.

PACS number: 74.25.Gz, 74.72.Dn, 78.30.-j

One and a half decades after the discovery of the superconductivity in cuprates, while substantial progress has been made, the underlying physics, especially the mechanism that leads to the high superconducting transition temperature (T_c), remains highly controversial. Therefore, it is legitimate to question whether some fundamental building blocks on which we have built our understanding of cuprate physics are incomplete or simply missing. In particular, we have examined the validity of the overwhelming single-component treatment, both theoretically and experimentally, of the doping-induced excess charges (hereafter holes) in the CuO_2 plane. In this report, we wish to establish this missing link by presenting clear experimental evidences for a unique composite picture of the charge system of cuprates.

In the past few years, charge and spin stripes [1] emerged as a possible topology of the charge inhomogeneity in the CuO_2 planes of the superconducting $\text{La}_{2-x}\text{Sr}_x\text{CuO}_4$ (LSCO). More recently the square lattice order with $p(4 \times 4)$ and $c(2 \times 2)$ symmetries was proposed as a plausible electronic structure of the bound holes [2, 3]. Most recently, evidences for an intrinsic superconducting [4] and non-superconducting [5] electronic phase separations were reported. Indeed, although the topology of the charge arrangements was not demonstrated, recent direct experimental evidences for charge inhomogeneities in the CuO_2 planes [6 - 8] seem to be consistent with the above observations. However, there has been no self-consistent far-IR single crystal work that clearly demonstrates the existence of such electronic phases. Only recently some far-IR results interpreted as charge density waves (CDW) [9] or charge stripes [10, 11] have been reported.

In this Letter, we report our findings of the far-IR signatures of the composite charge system of the free and bound holes. Through the in-plane (ab-plane) far-IR studies of a series of LSCO single crystals, we observed a screened plasma edge at the frequency (ω) between 15 cm^{-1} and 20 cm^{-1} , depending on the doping level. This local minimum in the ab-plane reflectivity comes from an extremely small free hole density (n_F) which is only $\sim 0.2 \%$ of the total holes. This small fraction of the holes are responsible for the nearly dissipationless normal state charge transport and superconductivity. We found that these free holes are massively screened by the rest of the holes condensed into electronic lattices (EL's) in the CuO_2 planes.

For the measurement of the ab-plane reflectivity we used high quality $\text{La}_{2-x}\text{Sr}_x\text{CuO}_4$ single crystals grown by the traveling-solvent floating-zone method with $x = 0.063, 0.07, 0.09, \text{ and } 0.11$. The growth and characterizations of the high crystal quality were reported elsewhere [12]. Both the dc resistivity and Meissner effect measurements of all four crystals are shown in Figure 1(a) and 1(b), respectively. The samples were prepared from pure, subgrain-free large as-grown ingots. The sample area was 5 mm in diameter and the angular error from the desired crystal axis was less than $\pm 1^\circ$.

We measured the reflectivity (R) at a near normal angle of incidence ($\sim 8^\circ$) on the sample. A Bruker 113v spectrometer is used to cover frequencies (ω 's) between 10 cm^{-1} ($\sim 1.2 \text{ meV}$) and 4000 cm^{-1} (0.5 eV) for the ab-plane R . As a reference, we used a gold (Au) mirror made by depositing Au film on a stainless steel mirror that had been polished under the same condition as the single crystal samples. We corrected the measured R in reference to the Au-mirror by multiplying the absolute R of the Au film calculated from the absolute measurement of the

surface resistance (r_s) of Au via $R = 1 - 4r_s$ [13]. In order to cover the ω 's below 20 cm^{-1} , we mounted a 75 micron Mylar beamsplitter and a composite Cu-doped Si-bolometer with 1 cm^2 active area operating at 2 K in conjunction with a parabolic light cone with a 7 mm diameter exit aperture. We controlled the sample temperature by directly monitoring the temperature (T) from the backside of the sample. We calculated the real part of the conductivity $\sigma_1(\omega)$ and the real part of the dielectric function $\epsilon_1(\omega)$ via a Kramers-Kronig transformation of R. We found that the asymptotic behavior of R below 12 cm^{-1} closely followed the Hagen-Rubens approximation. For high ω -extrapolation above 4000 cm^{-1} (0.5 eV), we used the data published by Uchida *et al.* for LSCO single crystals [14], which covers ω 's up to 37 eV.

In Figure 2, we present the unsmoothed far-IR ab-plane R (except for $\omega < \sim 13 \text{ cm}^{-1}$) of the four single crystal samples at various T. Overall R is high for all samples. As T decreases below 300 K, the R reaches a maximum at $\omega \sim 150 \text{ cm}^{-1}$ and then starts to decrease until it reaches a local minimum at around $\omega \sim 20 \text{ cm}^{-1}$ with decreasing ω . Near the local R minimum, there is a sharp peak(s) which grows as T decreases. The familiar phonons of the CuO_2 planes are readily seen in the R.

The corresponding Kramers-Kronig-derived $\sigma_1(\omega)$ plot in Figure 3 shows highly unexpected charge dynamics. There develops an intense asymmetric structure located at around $\omega \sim 120 \text{ cm}^{-1}$. This intense structure consists of a broad peak centered at $\omega \sim 60 \text{ cm}^{-1}$ and another stronger peak at $\omega \sim 90 \text{ cm}^{-1}$ as well as the doping enhanced ab-plane phonon modes at $\omega \sim 100 \text{ cm}^{-1}$, $\sim 140 \text{ cm}^{-1}$, and $\sim 200 \text{ cm}^{-1}$ [15]. In addition, a new mode (ω_{GL}) appears at $\omega \sim 18 \text{ cm}^{-1}$ for $x = 0.063$ ($T_c \sim 16 \text{ K}$). At low T, the $\omega_{\text{GL}} \sim 18 \text{ cm}^{-1}$ mode of $x = 0.07$ ($T_c \sim 20 \text{ K}$) sample takes over

the 22 cm^{-1} mode (ω_{GH}) seen at $T = 300 \text{ K}$ (see Figure 4) and below T_c , a new mode ($\omega_{\phi\text{L}}$) develops at $\sim 16 \text{ cm}^{-1}$. For $x = 0.09$ ($T_c \sim 28 \text{ K}$) sample, ω_{GH} mode is more pronounced and the development of the new mode $\sim 20 \text{ cm}^{-1}$ ($\omega_{\phi\text{H}}$) is evident at $T < T_c$. For $x = 0.11$ ($T_c \sim 30 \text{ K}$), there present both the ω_{GL} and ω_{GH} modes and the emergence of the new modes denoted as $\omega_{\phi\text{L}}$ and $\omega_{\phi\text{H}}$ at $T < T_c$ becomes much clearer. The $\omega_{\phi\text{L}}$ and $\omega_{\phi\text{H}}$ modes that appear only when $T < T_c$ are obviously related to the development of the superconducting state. These modes are assigned as the superconducting phase collective modes due to the broken longitudinal gauge symmetry [2]. The details of the T-dependence of the oscillator strength of the ω_{ϕ} 's and the ω_{G} 's are beyond the scope of this paper and will be reported later.

The $T = 300 \text{ K}$ $\sigma_1(\omega)$ and $\epsilon_1(\omega)$ for ω range between 10 cm^{-1} and 100 cm^{-1} are displayed in Figure 4. From the absence of a structure in $\sigma_1(\omega)$ at the zero-crossing in $\epsilon_1(\omega)$, it is clear that the local R minimum is the screened plasma edge of the free carriers in the CuO_2 planes. Note the extremely narrow Drude-like peak in $\sigma_1(\omega)$ with a half-width at half-maximum $\Gamma \sim 10 \text{ cm}^{-1}$ and the collective modes at $\omega \sim 18 \text{ cm}^{-1}$ and $\sim 22 \text{ cm}^{-1}$. Such a small Γ implies that the free holes in the CuO_2 planes transport charges without much dissipation in the normal state. It is this portion of the carriers that condenses into the superfluid state as evidenced by the disappearance of this Drude-like peak at $T \leq T_c$ (see the insets in Figure 3). From the measured dc conductivity and taking $\Gamma \sim 10 \text{ cm}^{-1}$, one can estimate the plasma frequency ω_p from $\omega_p^2 = 60\sigma_{\text{dc}}\Gamma$ to find $\omega_p \sim 388 \text{ cm}^{-1}$, 511 cm^{-1} , 542 cm^{-1} , and 612 cm^{-1} for $x = 0.063$, 0.07 , 0.09 , and 0.11 single crystals respectively. Here σ_{dc} is in $\Omega^{-1} \text{ cm}^{-1}$ and Γ in cm^{-1} . Comparing the above unscreened ab-plane ω_p with the screened plasma frequency $\omega_p^* = \omega_p / \sqrt{\epsilon_o}$ found from the zero crossing in $\epsilon_1(\omega)$, we

estimate the corresponding room temperature dielectric constant $\epsilon_0 \sim 890, 1348, 1198,$ and 1296 for $x = 0.063, 0.07, 0.09,$ and 0.11 respectively. From the unscreened ω_p 's, the known total hole concentrations, and using the free electron mass for the free holes, we find only $0.17\%, 0.25\%, 0.22\%,$ and 0.24% of holes are contributing to the charge transport at room temperature for $x = 0.063, 0.07, 0.09,$ and 0.11 respectively.

Since all the free carrier contribution is confined to $\omega < 20 \text{ cm}^{-1}$, it is clear that the high ab-plane R in the commonly accessed far-IR region is not due to the metallic behavior in the CuO_2 planes as usually assumed but due to the large imaginary part of the index of refraction arising from strong and rapidly varying absorption structures. Therefore, the measured R of cuprates at a finite angle of incidence is now sensitive to the angle of incidence and polarization of the far-IR [16] because the displacement current is dominating as often seen in the alkali halide crystals in the region between the transverse and longitudinal phonon modes. At our 8° angle of incidence, we found no difference between the measured R's with the π - and σ -polarized far-IR.

We point out that the $\sigma_1(\omega)$ below 100 cm^{-1} displayed in Figure 3 do not resemble any of the previously published normal state far-IR data [10, 15, 17 - 21] even though the presence of the intense electronic structure at $\omega \sim 120 \text{ cm}^{-1}$ is evident in their superconducting state $\sigma_1(\omega)$. The primary source of this problem lies in the experimental limitation on the angle of incidence, which is particularly important for cuprates. For example, at the 15° angle of incidence [15], instead of the decreasing reflectivity from the maximum at $\omega \sim 120 \text{ cm}^{-1}$ with decreasing ω as seen in this work, the reflectivity monotonically increases to ~ 0.95 at $\omega \sim 50 \text{ cm}^{-1}$ as if it follows

the free electron behavior. In a case of 8° angle incidence [11], a similar result as the present work was obtained except for the inconsistent T-dependence. Therefore, without the correct R information below 50 cm^{-1} , the tail on the high frequency side of the intense structure peaked at $\omega \sim 120 \text{ cm}^{-1}$ can easily be misidentified as the Drude-like tail because this structure also grows with doping [14, 15, 21]. Even at our 8° angle of incidence, the R for $\omega < \sim 15 \text{ cm}^{-1}$ and R at $\omega \sim 150 \text{ cm}^{-1}$ exceeds unity by $\sim 1 - 2 \%$ at low T, forcing us to rescale the overall R by matching the calculated Hagen-Rubens behavior. However, even though such scaling may decrease the magnitude of the background conductivity and the strength of the absorption peaks, all the spectral features were preserved.

In order to explain the above experimental observations of the massively screened free holes ($\sim 0.2 \%$ of the total holes) in the presence of the collective modes (ω_G 's), we conclude that the rest of the holes have to condense into an electronic lattice (EL) state to which the free carriers must be coupled. Furthermore, the free holes must "ride" the EL to avoid the scattering with the phonons of the CuO_2 lattice. Hence, we expect the single particle excitation gap (2Δ) in the $\sigma_1(\omega)$ of the EL which is the condensation energy of the holes into the EL state and the ω_G which is the gapped-Goldstone mode of the EL resulting from the strong hole-lattice interactions [22]. At the same time, the presence of ω_G gives $\epsilon_1(\omega)$ of the EL as $\epsilon_1^{\text{EL}}(\omega) = \epsilon_{\text{ab}} + \Omega_{\text{EL}}^2 / (\omega_G^2 - \omega^2) + \epsilon_1(2\Delta)$ [23]. Here ϵ_{ab} is the dielectric constant of the underlying CuO_2 lattice, $\epsilon_1(2\Delta)$ is the single particle excitation contribution, and Ω_{EL} is defined as $\Omega_{\text{EL}}^2 \equiv 4\pi n_{\text{EL}} e^2 / m_{\text{EL}}$ (n_{EL} = hole density and m_{EL} = dynamic mass of the EL).

From this ϵ_1^{EL} , one may estimate the dynamic mass of the bound holes in the EL state. For instance, using $\epsilon_1^{\text{EL}}(0) = \epsilon_0 \sim 890$ and $\omega_G \sim 18 \text{ cm}^{-1}$ and $n_{\text{EL}} \sim 6.3 \times 10^{20} \text{ holes/cm}^3$ (99.8% of the holes), we find $m_{\text{EL}} \sim 300 m_e$ ($m_e = \text{free electron mass}$) for $x = 0.063$ at 300 K. This small m_{EL} implies that the long-range order of the EL has already been sufficiently developed. For x beyond 0.063, the mode at $\sim 22 \text{ cm}^{-1}$ begins to dominate and develops stronger as the doping increases (see Figure 4). This new Goldstone mode must then be associated with a different EL state. The oscillator strength of the Goldstone mode continuously increases as T decreases below 300 K and saturates at $T \sim 200 \text{ K}$ by reaching the dynamic mass $\sim 180 m_e$ (details are not shown), indicating that the development of the long-range order of the EL's of $x = 0.063$ completes at $T \sim 200 \text{ K}$.

As a specific finger print, dimensionality of the EL structure determines the shape of the single particle excitation peak in $\sigma_1(\omega)$. If the EL has a one-dimensional structure, the square-root singularity in the joint-density-of-states would produce a sharp, asymmetric structure at $\omega = 2\Delta$ [23]. If it is two-dimensional, then the flat density-of-states would give rise to a step-like absorption feature at $\omega = 2\Delta$. In view of this, the $\sigma_1(\omega)$ shown in Figure 3 does not appear to bear the signature of the one-dimensional EL. Therefore, we suggest that the EL in the LSCO is two-dimensional in nature. Although the single particle excitation energy gap is not clearly seen owing to the two-dimensional nature of the EL and the presence of the intense peak at $\omega \sim 120 \text{ cm}^{-1}$, we do not expect this gap to be different from that of the polycrystalline LSCO samples ($2\Delta \sim 0.05 \text{ eV}$) [2, 3]. We suggest that the EL's in single crystalline LSCO are in random disorder state due to the randomly dispersed hard dopant [4] which would inhibit the development of the preferred EL's. Therefore, a variety of two-dimensional EL's may be possibly

inter-woven in LSCO single crystals. The extremely broad structure developed at around $\omega \sim 40$ cm^{-1} , which appears to be contributed by the modes at around $\omega \sim 30$ cm^{-1} and ~ 40 cm^{-1} lumped together with the broad structure at $\omega \sim 60$ cm^{-1} , reflects the influence of such electronic disorder. In this EL model, the broad peaks at $\omega \sim 60$ cm^{-1} and ~ 90 cm^{-1} are due to the optical transitions from the ground state of EL to the free hole state and from the free holes state to the excited EL state [2, 3].

In summary, based on our detailed far-IR studies of the LSCO single crystals, the ab-plane charge dynamics can be understood as a composite system consisting of a small fraction of free holes that move on the EL formed by the rest of the holes. We emphasize that the existence of free carriers and their transport are innately coupled to the underlying EL in this charge model unlike the common CDW system where the normal carriers are decoupled from the CDW condensate [24]. Our proposed charge model, if proven to be true, will place severe constraints on the microscopic model of the theory of high T_c superconductivity and serve as one of the fundamental building blocks for the interpretation of all the previous experimental observations.

We would like to acknowledge Mark Ankenbauer, Mark Sabatelli, and Bob Schrott for their fine machining work and Jiwu Xiong for her work in crystal growth and processing. PHH is supported by the State of Texas through the Texas Center for Superconductivity at the University of Houston. ZXZ, FZ, and WXT are supported by the Ministry of Science and Technology of China and National Science Foundation of China through Project G1999064601 and Project 10174090.

References

1. J.M. Tranquada *et al.*, Nature **375**, 561 (1995).
2. Y.H. Kim and P.H. Hor, Modern Physics Letter **B15**, 497 (2001).
3. P.H. Hor and Y.H. Kim, J. Phys.: Condens. Matter **14**, 10377 (2002).
4. B. Lorenz *et al.*, Phys. Rev. **B65**, 144522 (2002).
5. M. Matsuda *et al.*, Phys. Rev. **B65**, 134515 (2002).
6. I. Iguchi *et al.*, Nature **412**, 420 (2001).
7. S.H. Pan *et al.*, Nature **413**, 282 (2001).
8. P.M. Singer *et al.*, Phys. Rev. Lett. **88**, 047602 (2002).
9. C. Bernhard *et al.*, Solid State Commun. **121**, 93 (2002).
10. M. Dumm *et al.*, Phys. Rev. Lett. **88**, 147003 (2002).
11. F. Venturini *et al.*, Phys. Rev. **B66**, 060502 (2002).
12. F. Zhou *et al.*, to appear in “Superconductor Science & Technology”, preprint available at xxx.lanl.gov/abs/cond-mat/0212282.
13. G. Brändli and A.J. Sievers, Phys. Rev. **B5**, 3550 (1972).
14. S. Uchida *et al.*, Phys. Rev. **B43**, 7942 (1991).
15. M. Shimada *et al.*, Physica **C193**, 277 (1992) and references therein.
16. See, for example, M.V. Klein, *Optics* (John Wiley and Sons, New York, 1970), Chapter 11.
17. T. Timusk *et al.*, J. Phys. Chem. Solids **59**, 1953 (1998).
18. D.N. Basov *et al.*, Phys. Rev. Lett. **77**, 4090 (1996).
19. N.L. Wang *et al.*, Phys. Rev. **B59**, 576 (1999).
20. T. Startseva *et al.*, Phys. Rev. **B59**, 7184 (1999).

21. K. Takenaka *et al.*, Phys. Rev. **B65**, 092405 (2002).
22. Y.H. Kim *et al.*, Phys. Rev. **B36**, 7252 (1987).
23. P.A. Lee *et al.*, Solid State Commun. **14**, 703 (1974).
24. W. P. Beyermann *et al.*, Phys. Rev. Lett. **56**, 1489 (1986).

Figure Captions

Fig. 1. Plots of (a) the in-plane resistivity and (b) the field cooled (50e) measurements of $\text{La}_{2-x}\text{Sr}_x\text{CuO}_4$ single crystal samples for $x = 0.063, 0.07, 0.09$ and 0.11 with applied field along C-axis.

Fig. 2. Reflectivity spectra for $x = 0.063, 0.07, 0.09$ and 0.11 at various temperatures. $T = 8$ K (Black), 16 K (Blue), 24 K (Cyan), 30 K (Magenta), 50 K (Orange), 100 K (Dark Yellow), 200 K (Navy), and 300 K (Green). Note the common presence of the local minimum and the development of sharp structures near $\sim 20 \text{ cm}^{-1}$ for all the samples.

Fig. 3. The corresponding frequency-dependent conductivity calculated from the reflectivity in Figure 2. (a) For $x = 0.063$ ($T_c \sim 16$ K), there exists the collective mode (ω_{GL}) at $\sim 18 \text{ cm}^{-1}$. At $T < T_c$, the 18 cm^{-1} peak further increases its strength due to the presence of the phase collective mode ($\omega_{\phi\text{L}}$) at around 18 cm^{-1} . (b) In $x = 0.07$ ($T_c \sim 20$ K), the 22 cm^{-1} mode (ω_{GH}) is stronger than the 18 cm^{-1} mode (ω_{GL}) at room temperature (see Figure 4). For $T < T_c$, the phase collective mode ($\omega_{\phi\text{L}}$) develops at $\sim 16 \text{ cm}^{-1}$. (c) For $x = 0.09$ ($T_c \sim 28$ K), the development of the phase collective mode near 20 cm^{-1} ($\omega_{\phi\text{H}}$) is evident at $T < T_c$. (d) For $x = 0.11$ ($T_c \sim 30$ K), the separation among ω_{GL} , $\omega_{\phi\text{L}}$, ω_{GH} and $\omega_{\phi\text{H}}$ become clearer (see the text). Insets: The Drude-like tail of the $\sigma_1(\omega)$ and its disappearance at $T < T_c$ (Black: 8K; Magenta : 30K; Orange: 50 K). Olive curves below 10 cm^{-1} in the $\sigma_1(\omega)$ plot are calculated from the Drude model using the measured dc conductivity.

Fig. 4. Detailed comparison of the room temperature reflectivity with the corresponding $\sigma_1(\omega)$ and $\epsilon_1(\omega)$ (see the text). Red curves below 10 cm^{-1} in the $\sigma_1(\omega)$ plot are from the Drude fits. The Goldstone mode (ω_G) and the screened plasma frequency (ω_p^*) are indicated with an arrow. Note the same scale for both $\sigma_1(\omega)$ and $\epsilon_1(\omega)$.

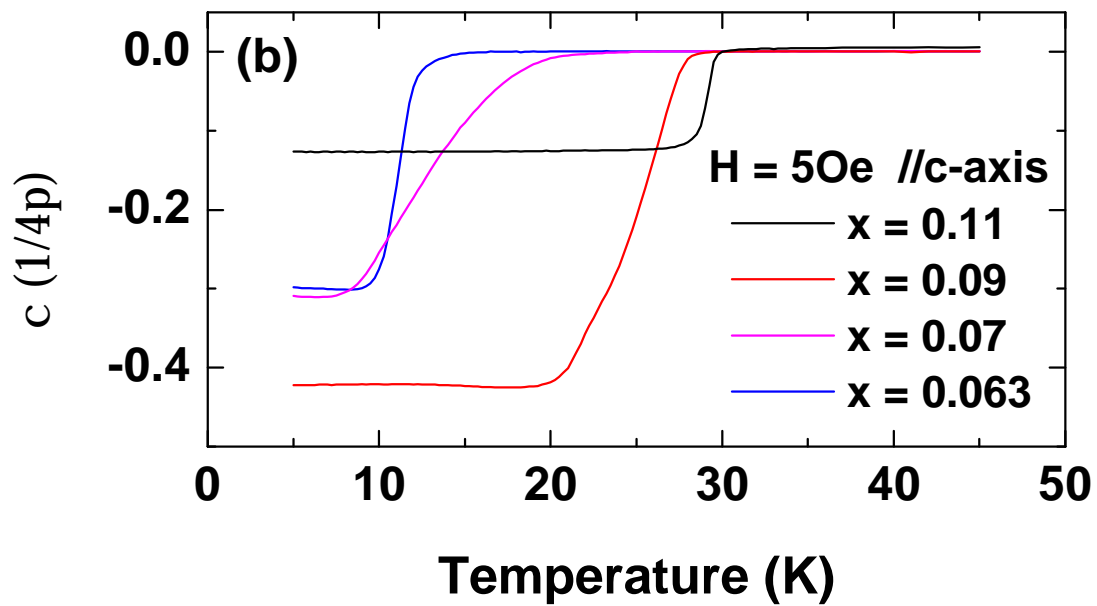
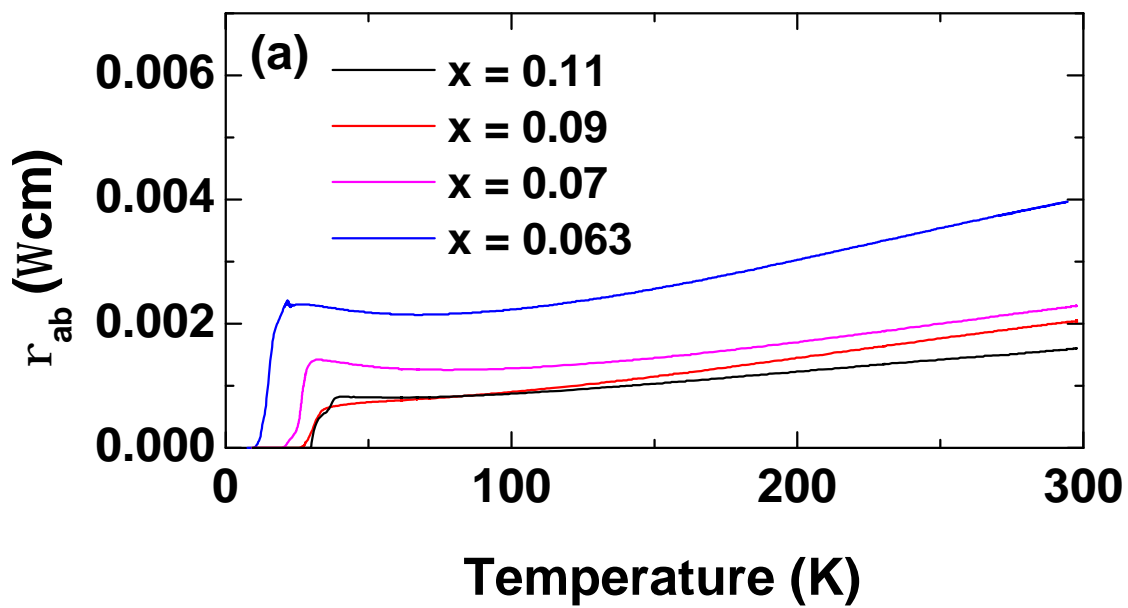


Figure 1

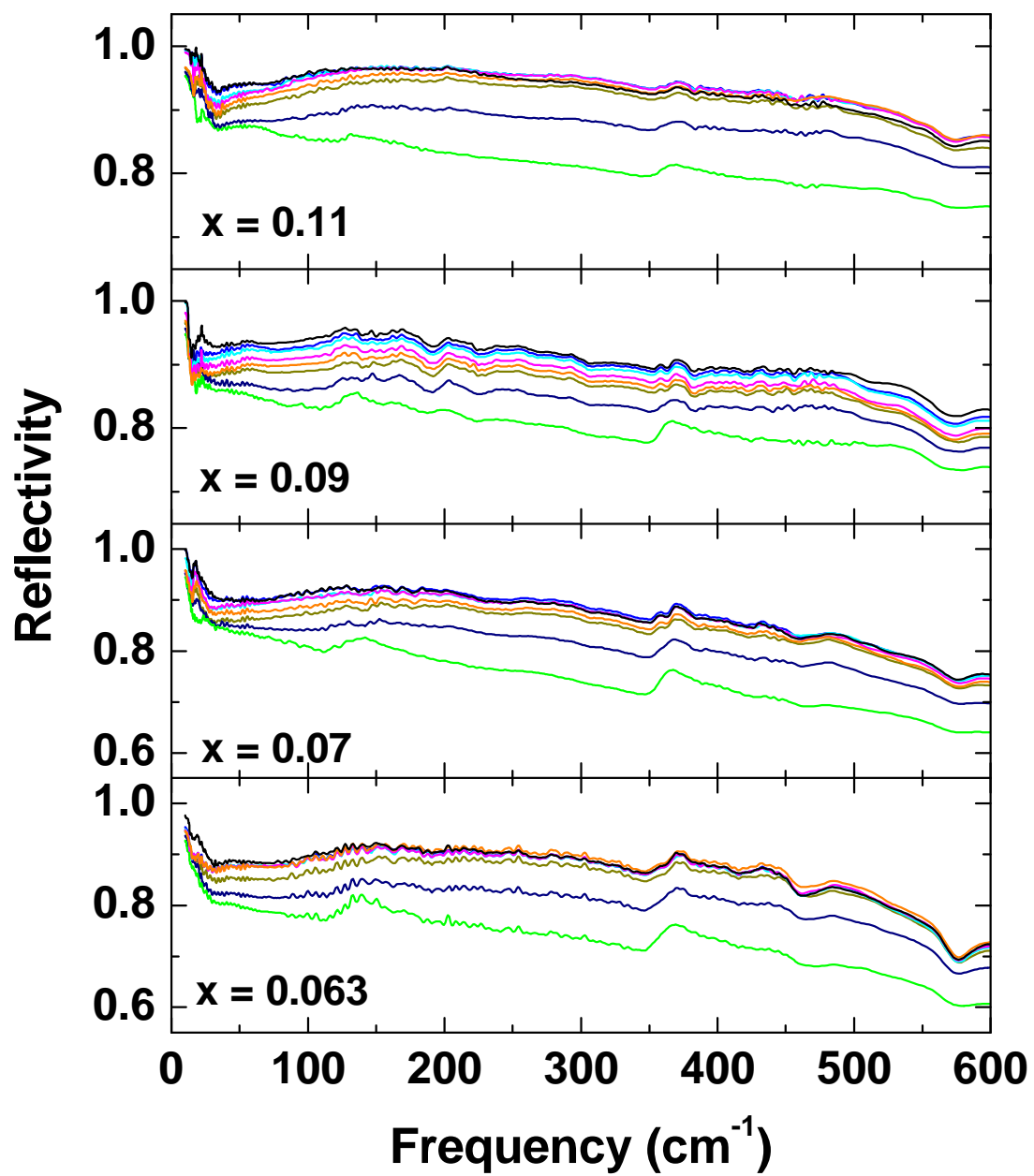


Figure 2

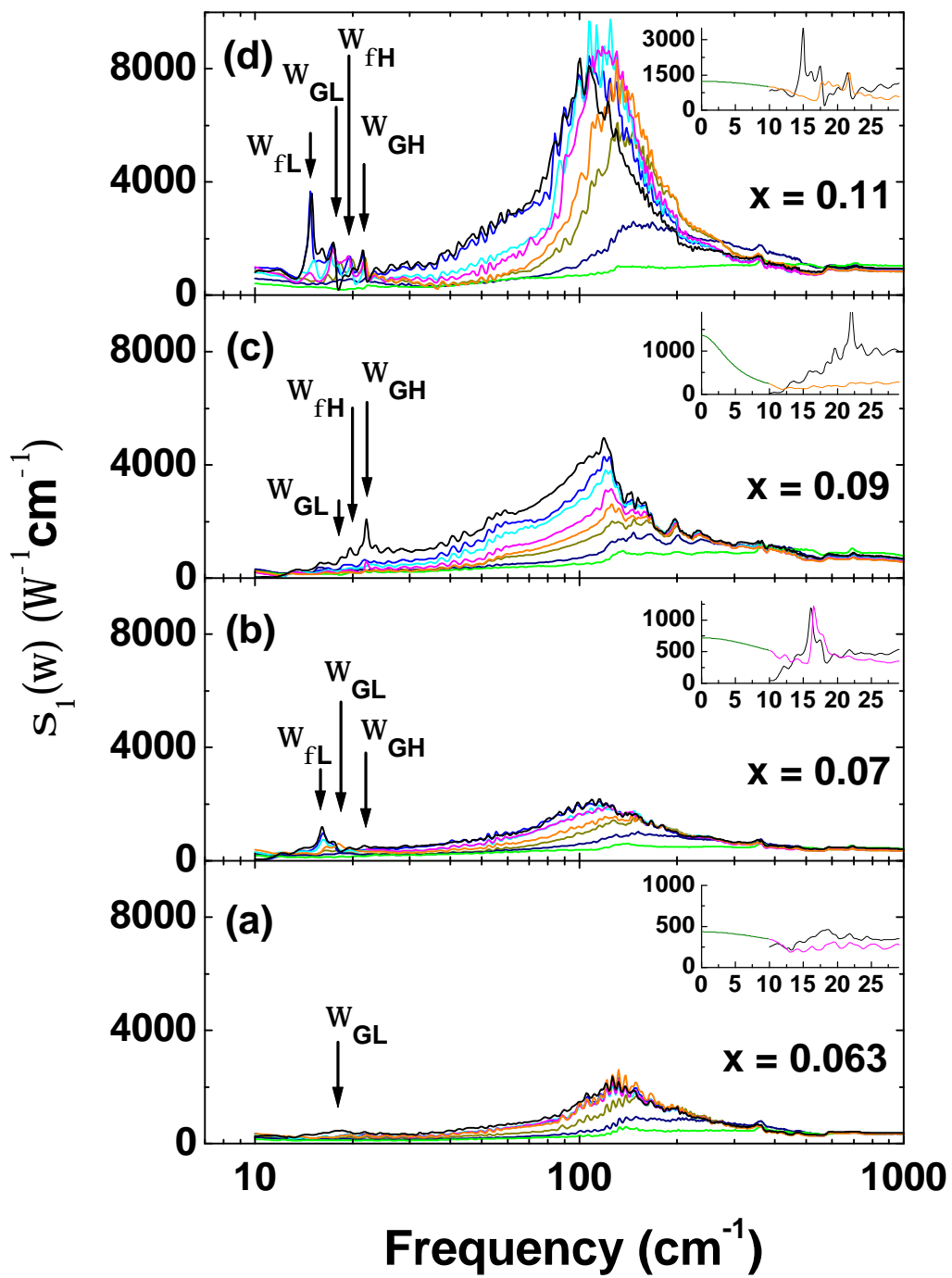


Figure 3

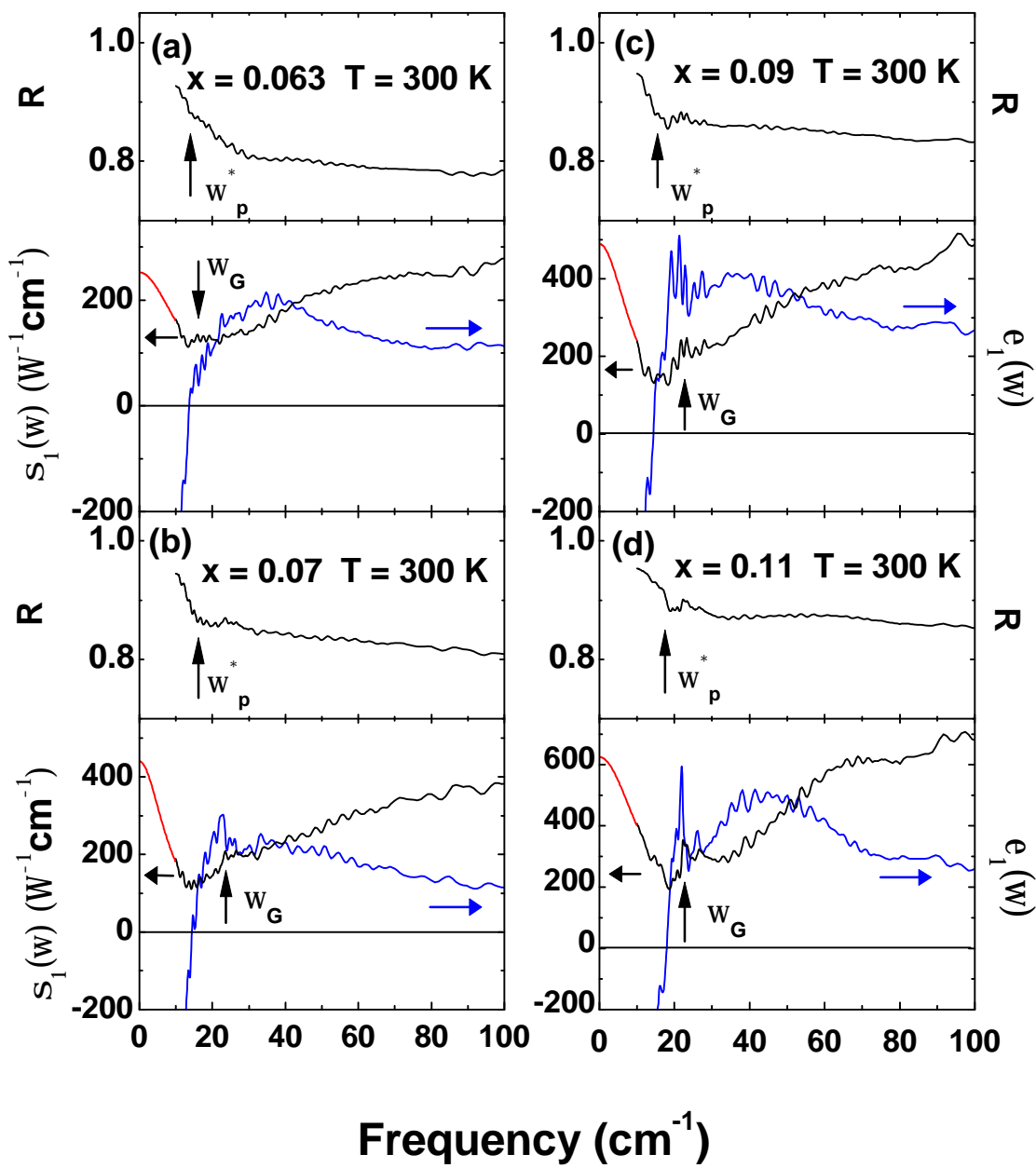


Figure 4